Global and Planetary Change 111 (2013) 43–56

Contents lists available at ScienceDirect

Global and Planetary Change

journal homepage: www.elsevier.com/locate/gloplacha

Rock magnetic properties and paleoenvironmental implications of an 8-Ma Late Cenozoic terrigenous succession from the northern Tian Shan foreland basin, northwestern China

Honghua Lu [a,b,*], Weiguo Zhang [c], Youli Li [d], Chenyin Dong [c], Tianqi Zhang [a], Zuyi Zhou [b], Xiangmin Zheng [a]

[a] College of Resources and Environmental Science, East China Normal University, Shanghai 200241, China
[b] State Key Laboratory of Marine Geology, Tongji University, Shanghai 200092, China
[c] State Key Laboratory of Estuarine and Coastal Research, East China Normal University, Shanghai 200062, China
[d] Key Laboratory of Earth Surface Processes of Ministry of Education, Peking University, Beijing 100871, China

ARTICLE INFO

Article history:
Received 4 November 2012
Received in revised form 9 August 2013
Accepted 12 August 2013
Available online 17 August 2013

Keywords:
Rock magnetism
Aridification
Late Cenozoic
Tian Shan
Asian inland

ABSTRACT

In the northern Tian Shan foreland basin, northwestern China, the thick Cenozoic terrigenous succession is crucial for paleoclimate–environmental reconstruction of the Asian interior. Here we present a detailed rock magnetic investigation on 245 samples from the ~1200-m-thick Neogene Taxi He section with a magnetostratigraphic age span of ca. 8.0 to 2.0 Ma in the northern Tian Shan foreland basin. Our rock magnetic results indicate that the significant variations in composition, concentration and grain size of magnetic minerals occurred at ca. 6.0, 3.7 and 2.7 Ma. The comparable compositions of rare earth elements (REEs) throughout the Neogene Taxi He section suggest no significant modification of the source materials during the interval between ca. 8.0 and 2.0 Ma, and thus sediment provenance is not regarded as responsible for these observed variations in rock magnetic properties. Our further analyses show that the variations in magnetic properties of the Taxi He section are casually linked mainly with lithofacies transition due to range encroachment into foreland basin as well as climate aridification. Identified enhancement of aridification was chronologically constrained at ca. 6.0 and 2.7 Ma. Such climate events are important archives for reconstructing the Late Cenozoic paleoclimatic history of the Asian interior. Further comparison between different paleoclimate records clearly indicates that magnetic parameters such as S_{-100mT} are potentially effective proxy indices for paleoclimate–environmental reconstruction in the Tian Shan foreland basins and the nearby areas.

1. Introduction

The Asian inland is characterized by exceptional topographic relief and widespread deserts and semi-deserts (Fig. 1a). Its environmental evolution during the late Cenozoic is featured by two processes: (1) growth and uplift of the Tibetan Plateau (including the hinterland to the north) and (2) stepwise development of dry climate. Many investigations have attempted to reconstruct the process of plateau uplift (e.g., Li and Fang, 1998; Zheng et al., 2000; Kirby et al., 2002; Fang et al., 2005; Clark et al., 2005; Charreau et al., 2005, 2006; Lu et al., in press) or constrain the aridification history (e.g., Sun and Zhang, 2008; Huang et al., 2010; Sun et al., 2010, 2011; Chang et al., 2012; Miao et al., 2013; Zhang et al., 2013). The relative role of the Tibetan Plateau uplift and Cenozoic global cooling in the aridification process of the Asian interior, however, remains an issue of debate (e.g., Dupont-Nivet et al., 2007; Miao et al., 2012). This is in part due to the fact that paleoenvironmental records from this region are still quite limited, considering such a broad area of the Asian inland including arid and semi-arid northwestern China (Fig. 1a). Furthermore, different paleoenvironmental proxy data (e.g., palynology, geochemistry, rock magnetism, sediment-accumulation rate, etc.) from different areas might lead to contradictory results due to imprints of local settings and different recording mechanisms. Therefore, more detailed paleoclimatic/tectonic investigations over a broad area should be beneficial to paleoenvironmental reconstruction of the Asian interior.

The east–west trending Tian Shan range, separating the Junggar Basin to the north from the Tarim Basin to the south (Fig. 1a), lies about 2000 km north of the initial India–Asia collision front. In response to the India–Asia collision during the early Cenozoic (Najman et al., 2001), the Tian Shan range has been tectonically reactivated and uplifted and intensely extended into its both northern and southern foreland basins (e.g., Molnar and Tapponnier, 1975; Avouac et al., 1993). The uplifted topography and changed geomorphic patterns

* Corresponding author at: College of Resources and Environmental Science, East China Normal University, Shanghai 200241, China. Tel.: +86 21 54341240.
E-mail address: hhlv@geo.ecnu.edu.cn (H. Lu).

0921-8181/$ – see front matter © 2013 Elsevier B.V. All rights reserved.
http://dx.doi.org/10.1016/j.gloplacha.2013.08.007

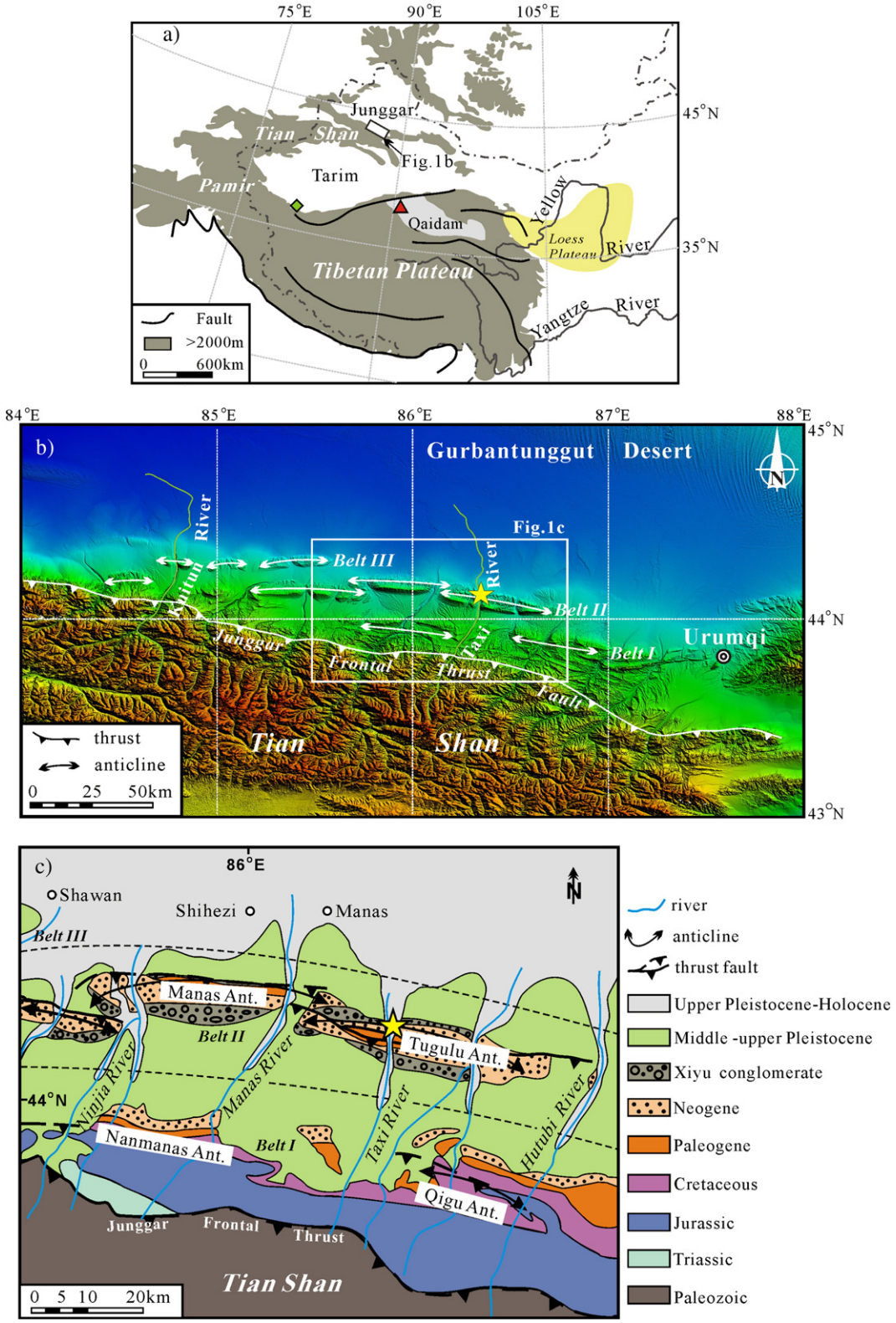

Fig. 1. (a) Map shows overall topographical pattern and tectonic setting of the interior of Asia. Prismatic and triangle show location of Sun et al.'s (2008) and Miao et al.'s (2013) sections, respectively, which are compared in Fig. 11. (b) Digital elevation model (DEM) map of the northern Tian Shan foreland showing tectonic setting. (c) Mesozoic and Cenozoic depositional strata exposed in structural belts. Stars in (b) and (c) indicate the location of the studied Taxi He section.

have caused Cenozoic environmental change within the Tian Shan range and its surrounding area (e.g., Cui et al., 1998), which is documented in the terrestrial sediments shed from the range and deposited in its intramontane and foreland basins. Studying this Cenozoic terrigenous succession is thus of great importance for better understanding regional environmental change and its possible relationship with uplift

and growth of the Tibetan Plateau and the hinterland to the north (e.g., the Tian Shan range) as well as global climate change.

Rock magnetism has been successively used in tracking past changes in climate (e.g., Deng et al., 2005; Fang et al., 2007; Zhang et al., 2009; Huang et al., 2010; Chang et al., 2012) and regional tectonics (e.g., Gilder et al., 2001; Sun et al., 2005; Charreau et al., 2006; Lu and Xiong, 2009; Zhang et al., 2012) recorded in loess–paleosol sequences, lake and marine sediments. However, a systematic rock magnetic paleoenvironmental investigation on the late Cenozoic terrigenous sediments is still quite limited in the northern Tian Shan foreland, northwestern China, which is in great contrast to the magnetostratigraphic works there. Here we present the results of detailed rock magnetic investigations on the ~1200 m-thick Neogene Taxi He section (He means "river" in Chinese) from this foreland basin (Fig. 1b and c). The goals of this paper are (1) to reveal rock magnetic properties of the upper Cenozoic terrigenous sequence at the Taxi He area and (2) to discuss its paleoclimate implications. An earlier work on rock magnetism of the Cenozoic terrigenous succession at the present study area has been conducted by Li et al. (2006). Their results show that magnetic mineralogy is controlled by lithofacies (Li et al., 2006). However, limited samples (only 18 samples measured) were not enough to reveal the temporal variations in rock magnetic properties and hence probe into its controlling factors and paleoenvironmental implications. Nevertheless, the results of Li et al. (2006) do provide useful background information for the rock magnetic studies presented in this study.

2. General setting and stratigraphy

The Tian Shan, stretching ~2500 km from east to west, is one of the largest and most active mountain ranges in Central Asia. The average elevation of ridges along the range is ~4000 m above sea level, while the highest peak Tuomer exceeds 7400 m. Most of rivers in the piedmonts of the Tian Shan range originate from active glaciers in the axial parts of the range and carry sediments eroded from the range to its foreland basins. With an annual precipitation of <300 mm/yr in the piedmonts, the fluvial water supply depends strongly on snow melt, and thus displays strong seasonal variations in discharge (Lu et al., 2010a). Similarly, discharge, sediment transport and erosional competency of these piedmont river systems likely varied in response to past climate change (Lu et al., 2010a). Pleistocene eolian loess extensively mantles several old fan and high terrace surfaces developed by these piedmont fluvial systems, as well as dissected anticlines in the north piedmont of the Tian Shan (Zhang, 1981; Deng et al., 2000; Lu et al., 2010a). This loess deposition has been casually linked with the aridification of the Junggar Basin and the development of the Gurbantunggut Desert in the center of this basin (Fang et al., 2002), which is the second largest desert in China and covers an area of 48,800 km^2 with the elevation ranging from about 300 to 600 m.

The modern Tian Shan has been built by basinward thrusting along faults as a result of the north–south convergence in Central Asia during the early Cenozoic (e.g., Avouac et al., 1993; Zhang et al., 1996). We focus on the northern Tian Shan foreland, where three thrust-fold belts (traditionally known as Belts I to III) stretch from the mountain front sequentially towards the foreland basin and characterize the regional topography (Fig. 1b and c). Along a traverse from the proximal to distal structure belts, growth strata and unconformities chronologically constrain their initial growth to range sequentially from Miocene to Mio-Pliocene to latest Early Pleistocene (Lu et al., 2010b). Most anticlines in these structural belts comprise Cenozoic depositional strata, except for some anticlines of zone I that expose both Mesozoic and Cenozoic strata (Fig. 1c). North-flowing piedmont rivers incise these piedmont anticlines perpendicular to strike where they expose thick successions of Cenozoic or even Mesozoic deposits (Fig. 1c).

The studied Taxi He section is located on the northern limb of the Tugulu Anticline in thrust-fold Belt II along the northern Tian Shan foreland (Fig. 1b and c). The section is ~1,200 m in thickness and comprises three formations from the base to the top: the Taxihe, Dushanzi and Xiyu Formations (BGMRX, 1993) (Fig. 2). The Taxihe Formation primarily comprises muddy siltstone and mudstone beds interbedded occasionally with coarse-grained sandstone or conglomerate sediments (Fig. 2d). The Dushanzi Formation consists dominantly of siltstone, sandstone, and conglomerate beds (Fig. 2b and c). The Xiyu Formation typically comprises a thick sequence of alluvial gravels, in which some brownish interbedded sandy or silty lenses are found, especially in the lowermost part of this formation (Fig. 2a). On the whole, the Taxi He section can be divided into two lithofacies units: (1) fine-textured shallow lacustrine sediments between depths of 1200 and ~800 m and (2) coarse-grained alluvial fan deposits between ~800 and 0 m (Fig. 2) (Lu et al., 2010b). Our previous paleomagnetic investigation (Lu et al., 2010b) has chronologically constrained the range of the Taxi He section from ca. 8.0 to 2.0 Ma (Fig. 2), within which we analyze the temporal changes of a suite of rock magnetic parameters of the Neogene Taxi He sediments and discuss its paleoclimate implications.

3. Materials and methods

In the Taxi He section, samples were taken from each sampled horizon with the average interval of ~4 m. Most samples were collected from mudstone or siltstone beds. Where the deposits are predominantly conglomeratic, sampling was conducted on thin lenticular beds of silty or sandy sediments. A total of 245 samples were collected from the section for the following rock magnetic measurements. In the laboratory, all the samples were cut into ~2.0-cm long cylinders that were 2.5-cm in diameter. When needed, the dried sediment was disaggregated in an agate mortar.

Bulk volume magnetic susceptibility (κ) was measured using a Bartington MS2B dual frequency magnetic susceptibility meter at two frequencies (low and high frequencies are 0.47 and 4.7 kHz, respectively). Anhysteretic remanent magnetization (ARM) was acquired in a peak alternating field (AF) of 100 mT with a bias field of 40 μT using a Dtech 2000 demagnetizer. Isothermal remanent magnetization (IRM) was acquired after imparting a field at 1 T using a MMPM10 pulse magnetizer, and then applying backfields at −100 mT and −300 mT. IRM obtained at 1 T is referred to as saturation IRM (SIRM), and those in the backfield of −100 mT and −300 mT as IRM_{-100mT} and IRM_{-300mT}. Remanent magnetization was measured using a Molspin spinner magnetometer. We then calculated mass-specific magnetic susceptibility at low frequency (χ_{lf}) and high frequency (χ_{hf}), χ_{ARM}, SIRM and other parameters according to these values, including frequency-dependent susceptibility (χ_{fd}%), χ_{ARM}/χ_{lf}, S_{-100mT} and S_{-300mT}. Frequency-dependent susceptibility was calculated as $\chi_{fd}\% (=[(\chi_{lf} - \chi_{hf}) / \chi_{lf}] \times 100)$ in percentage form. χ_{ARM} is expressed as susceptibility of ARM. S_{-100mT} and S_{-300mT} were calculated as $S_{-100mT} = [(SIRM - IRM_{-100mT}) / (2 \times SIRM)] \times 100$ and $S_{-300mT} = [(SIRM - IRM_{-300mT}) / (2 \times SIRM)] \times 100$ (Yu and Oldfield, 1989), respectively. Selected samples were further subjected to hysteresis loop measurements and IRM demagnetization using a Variable Field Translation Balance (VFTB). Saturation magnetization (Ms), saturation remanent magnetization (Mrs), coercive force (Bc) and coercivity of remanence (Bcr) were then determined according to hysteresis loop and IRM demagnetization curves. Detailed IRM acquisition curves (10 mT to 7 T) for selected samples were obtained using a MMPM10 pulse magnetizer. IRM component analysis was carried out following the method by Kruiver et al. (2001). Thermal magnetic analysis (κ–T) was conducted using a MFK1-FB Kappabridge equipped with a CS-4 high-temperature furnace in an argon atmosphere. All these rock magnetic measurements have been performed at the State Key Laboratory of Estuarine and Coastal Research of East China Normal University in Shanghai.

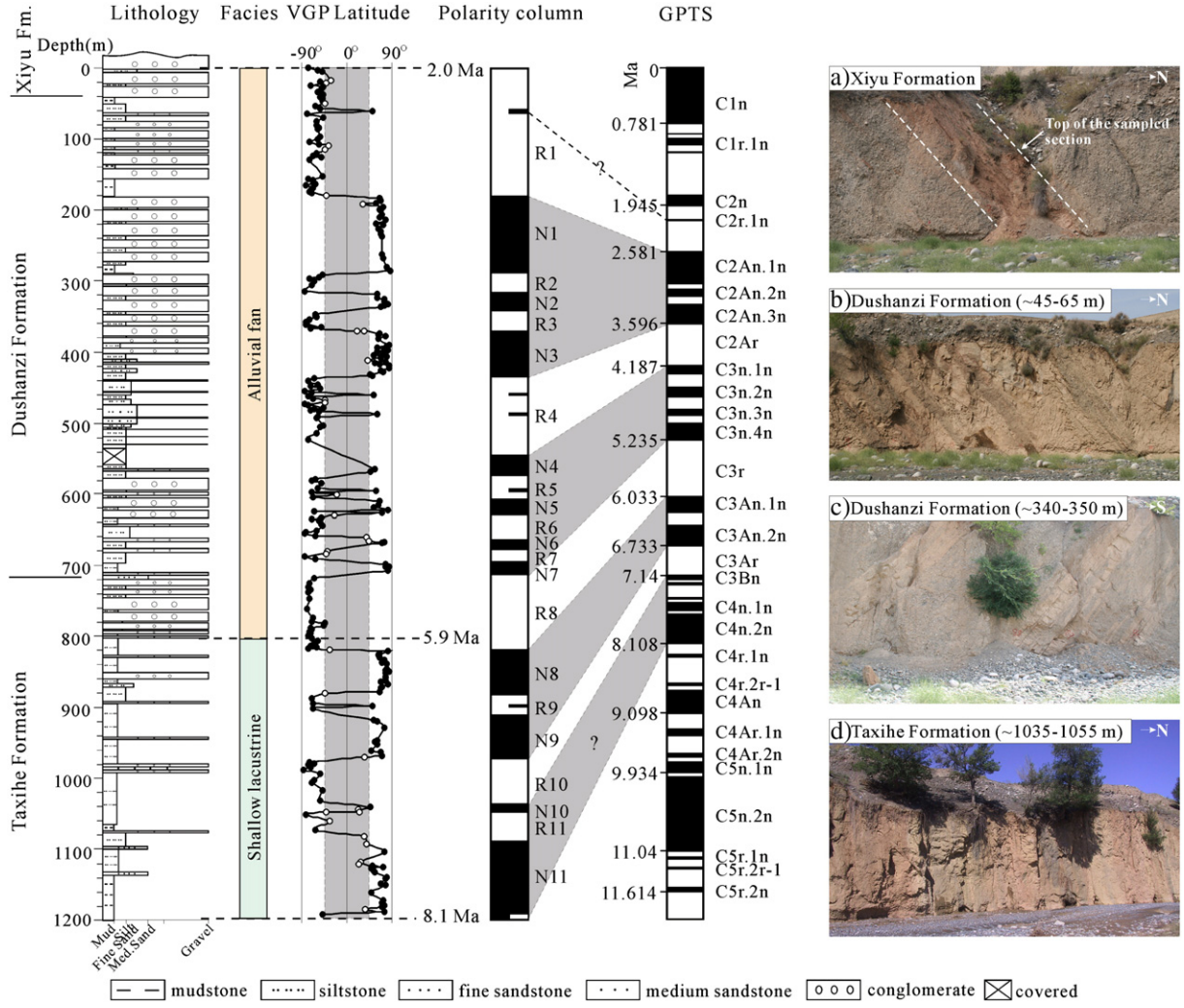

Fig. 2. Lithology, sedimentary facies, and magnetic polarity stratigraphy (MPS) of the Taxi He section. The correlation of MPS with the geomagnetic polarity time scale (GPTS) of Lourens et al. (2004) constrains the age span of the section from ca. 8.0 to 2.0 Ma (Lu et al., 2010b). Photos show representative lithofacies of different stratigraphical levels in the Taxi He section. a: coarse-grained alluvial conglomerates with some brownish interbedded sandy or silty lenses. b–c: alternation of siltstone, sandstone, and conglomerate beds in the Dushanzi Formation. d: dominance of shallow lacustrine muddy siltstone and mudstone in the Taxihe Formation. The depth interval of each photo is after the formation name.

Nineteen selected samples were subjected to analysis of rare earth elements (REEs) using a VGX7 inductively coupled plasma emission mass spectrometry (ICP-MS) at the State Key Laboratory of Marine Geology of Tongji University in Shanghai. The procedure for REE analysis is after that of Shao et al. (2010). Three international and China reference standards (GSR5, GSR6 and GSD9) were used to ensure analysis quality, and the precision and accuracy of the analysis was better than 2%.

For 237 samples from the sampled horizons, particle size distribution was measured at the State Key Laboratory of Estuarine and Coastal Research of East China Normal University in Shanghai. After removal of organic matter and carbonates with 5% H_2O_2 and 0.2 M HCl, the samples with addition of 0.5 M $(NaPO_3)_6$ were subjected to ultrasonic dispersion. The particle size distribution of the well-dispersed samples were then measured with the LS 13 320 Laser Diffraction Particle Size Analyzer, which has a measuring range from 0.04 μm to 2000 μm.

4. Results

As shown in Fig. 3, rock magnetic parameters display significant variations at ages of ca. 5.9, 3.7, and 2.7 Ma. Correspondingly, the Taxi He section is divided by these three ages into four layers: Layer 1 (1200–800 m with an assigned magnetostratigraphic age of ca. 8.0–5.9 Ma), Layer 2 (~800–460 m with an age of ca. 5.9–3.7 Ma), Layer 3 (~460–220 m with an age of ca. 3.7–2.7 Ma), and Layer 4 (~220–0 m with an age of ca. 2.7–2.1 Ma). In these four layers are observed significant variations in magnetic mineralogy, concentration and grain size.

4.1. Magnetic mineralogy

S_{-300mT} serves as a measure of the relative importance of low- (e.g., magnetite) and high-coercivity (e.g., hematite and goethite) components in the total assemblage (Bloemendal and Liu, 2005), while S_{-100mT} reflects the ratio of low-coercivity minerals to medium- and high-coercivity minerals (Yamazaki, 2009; Yamazaki and Ikehara, 2012). The medium-coercivity components include maghemite or soft hematite (Thompson and Oldfield, 1986; Robinson and Sahota, 2000; Zhang et al., 2007; Yamazaki, 2009). The absence of significant correlations between S_{-300mT} and sediment particle size in the Taxi He section (Fig. 4a, b and c) implies that S_{-300mT} is independent of sediment particle size. Throughout the section, the S_{-300mT} ratio is generally greater than 90% but less than 95% (Fig. 3j), indicating the dominance of magnetic properties by ferrimagnetic minerals (e.g., magnetite) together with contribution of antiferromagnetic minerals (e.g., hematite). In Layer 1,

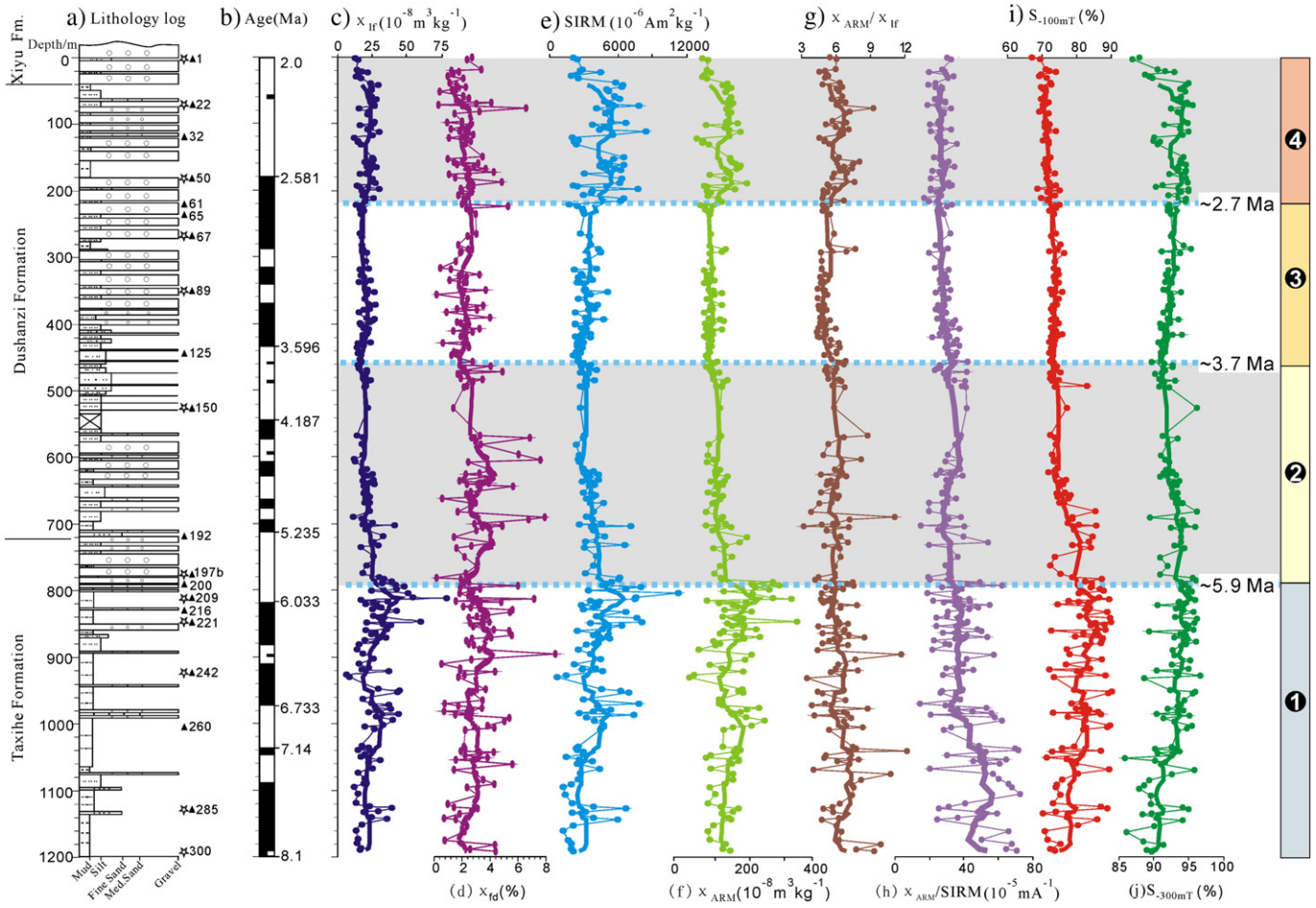

Fig. 3. Lithology, magnetostratigraphy, and rock magnetic results of the Taxi He section. (a) Lithology log, (b) magnetostratigraphic chronology (Lu et al., 2010b), (c) low-frequency magnetic susceptibility (χ_{lf}), (d) frequency-dependent magnetic susceptibility (χ_{fd}%), (e) saturation isothermal remanent magnetization (SIRM), (f) anhysteretic remanent magnetization (χ_{ARM}), (g) χ_{ARM}/χ_{lf}, (h) χ_{ARM}/SIRM, (i) S_{-100mT} ratio, and (j) S_{-300mT} ratio. Four layers, Layers 1 to 4, are recognized according to the variations in these magnetic parameters. Open stars (twelve) and solid triangles (nineteen) besides the lithology log show the stratigraphic positions of the samples subjected to thermomagnetic and hysteresis loop measurements and geochemical analysis, respectively. Thick solid line in (c) to (j) shows the 10-point moving average of each magnetic parameter.

S_{-300mT} shows an upward increasing trend, followed by a trend of upward declining values in Layer 2 (Fig. 3j). Subsequently, the S_{-300mT} ratio in Layers 3 and 4 begins to increase from ~90% to ~95% till ca. 2.1 Ma (Fig. 3j). Although S_{-100mT} shows a similar trend with S_{-300mT} in Layers 1 and 2, this ratio displays an opposite variation pattern in Layers 3 and 4 (after ca. 3.7 Ma), i.e., a long-term trend of up-section decrease from ~75% to ~70% (Fig. 3i). This suggests that although proportions of ferrimagnetic minerals increase toward the top of the section shown by the S_{-300mT} ratio (Fig. 3j), the proportion of the medium-coercivity component increases upward as shown by declining S_{-100mT} values in Layers 3 and 4.

Thermal magnetic measurements further confirm the dominance of magnetic properties by ferrimagnetic minerals. The obvious decrease in κ–T curves at about 600 °C or even higher suggests that partially oxidized magnetite or maghemite is the main magnetic carrier (Fig. 5a). The heating curves for all the samples display an inflection between 300 and 450 °C (Fig. 5a), which is generally ascribed to the conversion of maghemite to hematite (Liu et al., 2005; Li et al., 2006). In the same temperature interval, the samples from the upper part of the Taxi He section exhibit more decreases in susceptibility (Fig. 5a). The cooling curves for samples from the uppermost part of the section display an obvious increase in magnetic susceptibility and go higher than the heating ones (Fig. 5a), which is likely due to a decomposition of clay minerals and the formation of new magnetic minerals (e.g., Zuo et al., 2012). An unnegligible decrease in susceptibility, however, is also observed between ~600 and 680 °C (Fig. 5a), possibly suggesting the existence of hematite (e.g., Zhu, 2005). The hysteresis loops become almost closed beyond 300 mT (Fig. 5b), and exhibit slightly higher Bc values in samples with higher Bcr values (Fig. 5b and c). It is also evident that samples with higher Bcr values correspond to a larger decrease of magnetic susceptibility in the 300–450 °C range on the heating curves (Fig. 5), suggesting that a higher Bcr is linked to the presence of maghemite.

Typical IRM acquisition curves are presented in Fig. 6. In general, two high coercivity components with mean coercivity ($B_{1/2}$) as 400–800 mT and >2000 mT can be identified and interpreted to be hematite and goethite, respectively (Kruvier et al., 2001). The lowest coercivity component has $B_{1/2}$ as ~28–45 mT, and the medium coercivity component has $B_{1/2}$ as ~130–160 mT. In the study of Chinese loess–paleosol sequences, a similar coercivity component has been found, and it is suggested to be detrital maghemite or titanomagnetite (Hu et al., 2013). Clearly, sediments with higher Bcr values contain a higher contribution from the medium coercivity component (Fig. 6). Combined with the thermal magnetic evidence (Fig. 5), we suggest that the medium component be maghemite.

4.2. Magnetic mineral concentration

χ_{lf} and SIRM are commonly used as approximate indicators of magnetic mineral concentration, especially ferrimagnetic minerals (e.g., magnetite) (Thompson and Oldfield, 1986). In comparison to χ_{lf},

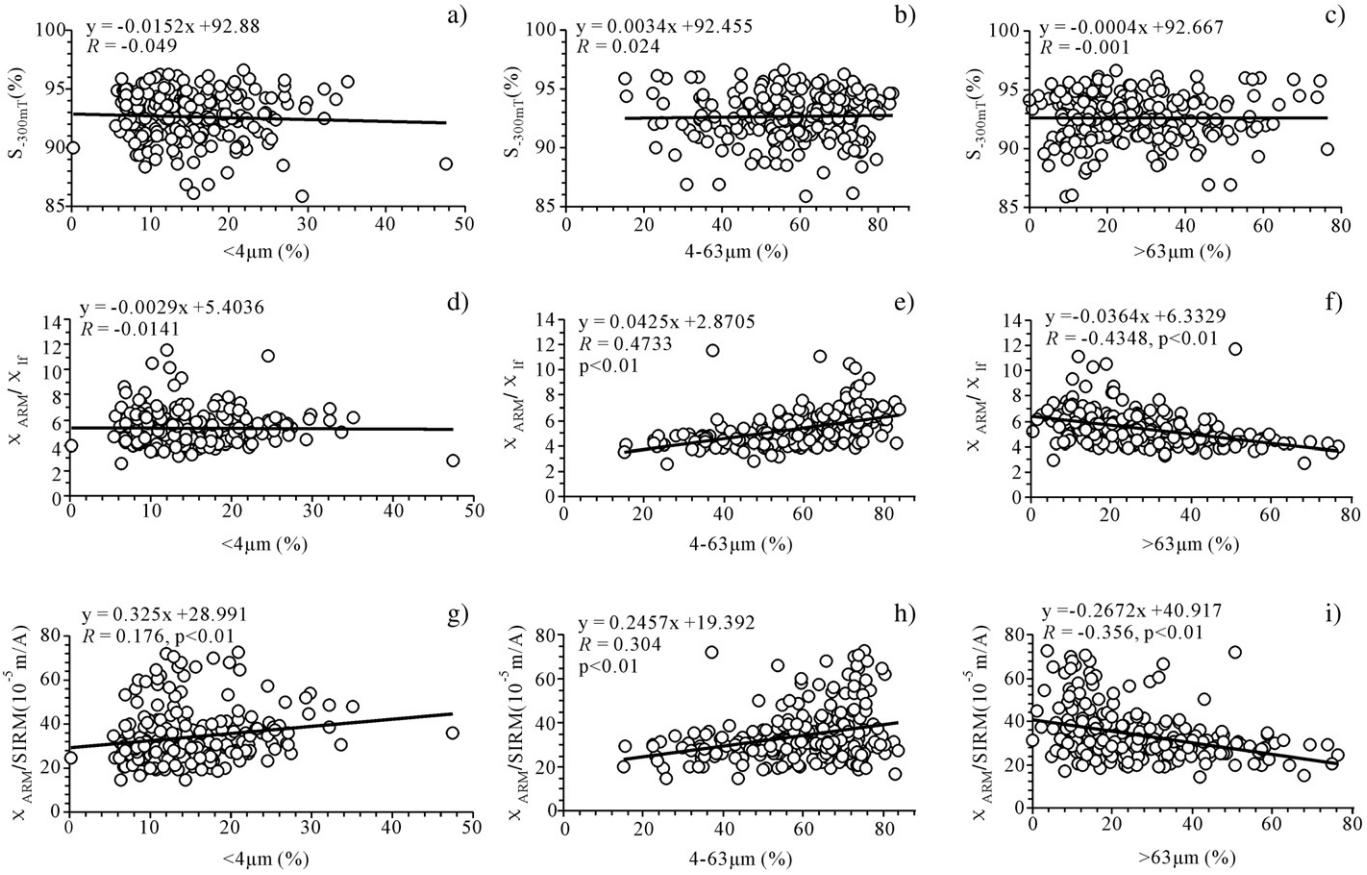

Fig. 4. Correlations between rock magnetic parameters (S_{-300mT}, χ_{ARM}/χ_{lf} and χ_{ARM}/SIRM) and sediment particle size (clay fraction of <4 μm, silt fraction of 4–63 μm and sand fraction of >63 μm) for 237 samples from the Neogene Taxi He section. The correlations are insignificant for cases a, b, c and d; the relationships for cases e, f, h and i are significant. Relatively, the correlation for case g is weaker. The p value is shown only for the significant relationships.

SIRM is unaffected by (super)paramagnetic and diamagnetic minerals (Thompson and Oldfield, 1986). Given that a significant relationship exists between χ_{lf} and SIRM (Fig. 7a), the χ_{lf} signals are thought to be dominated mainly by ferrimagnetic minerals. Fig. 3c shows χ_{lf} as a function of depth for the Taxi He section, where the χ_{lf} values range from ~7 to ~80 × 10^{-8} m^3/kg with an average of 23 × 10^{-8} m^3/kg. It is clear that the χ_{lf} values before ca. 5.9 Ma display an overall trend of up-section increase from ~20 to ~50 × 10^{-8} m^3/kg despite several fluctuations within the depth intervals of 940 to 780 m and 1040 to 940 m in Layer 1 (Fig. 3c), followed by a weakly declining-upward trend till ca. 3.7 Ma (Fig. 3c). The χ_{lf} values of the overlying sediments begin to increase slightly upward, especially in Layer 4 (Fig. 3c). SIRM shows a slightly upward increasing trend in Layer 1, followed by a trend of declining values in Layer 2 (Fig. 3e). Subsequently, SIRM in Layers 3 and 4 begins to increase till ca. 2.1 Ma (Fig. 3e).

χ_{ARM} is particularly sensitive to single domain ferrimagnetic grains (King et al., 1982; Maher, 1988). When plotted as a function of depth, the χ_{ARM} value generally follows that of SIRM. It shows a progressive increasing trend in Layer 1, followed by a long-term decreasing trend in Layers 2 and 3. At the 220-m depth, the χ_{ARM} values jump to a relatively high level in Layer 4 (Fig. 3f). Like SIRM, a significant relationship is also observed between χ_{ARM} and χ_{lf} (Fig. 7b).

4.3. Magnetic mineral grain size

χ_{fd}% can be used to detect the relative contribution of ultra-fine grains spanning the super-paramagnetic (SP)/single domain (SD) transition boundary to the total assemblage of magnetic minerals (Thompson and Oldfield, 1986). For χ_{fd}% values <5%, grains larger than SP are dominant, whereas SP grains dominate when χ_{fd}% is greater than 5% (Dearing, 1999). In the Taxi He section, although several samples between ~700 and ~550 m display the χ_{fd}% values higher than 5% and even exceeding ~7–8% (Fig. 3d), 85% samples display χ_{fd}% values <4%, suggesting that SP grains are not dominant in magnetic mineral assemblages (Thompson and Oldfield, 1986). Furthermore, there is a slight long-term decrease of χ_{fd}% from about 4% to about 2% in Layers 2 to 4 (Fig. 3d), suggesting decreased proportions of SP grains upward. All measured samples fall in the pseudo-single-domain (PSD) region on the Day plot (Day et al., 1977; Dunlop, 2002) (Fig. 8), implying that PSD grains or SD-MD (multi-domain) mixtures are the dominant grain size of magnetic minerals in the Taxi He sediments. Moreover, sediments from the upper part of the section are shifted to higher Bcr/Bc values (Fig. 8), which may indicate the presence of harder magnetic components, consistent with the thermal magnetic (Fig. 5) and IRM unmixing results (Fig. 6).

The χ_{ARM}/χ_{lf} ratio has been proposed as a grain size indicator (Banerjee et al., 1981), which decreases with increasing grain size. But this ratio is also affected by the concentration of SP grain, being reduced when SP grain is dominant in magnetic mineral grain composition. Considering the modest presence of SP grains in the Neogene Taxi He sediments indicated by low χ_{fd}% values (Fig. 3d), the χ_{ARM}/χ_{lf} ratio in this section is not strongly influenced by SP grains. In Layers 1 to 2, a long-term trend is apparent with higher χ_{ARM}/χ_{lf} ratios at the base of the section going to lower ratios till ca. 3.7 Ma, indicating a coarsening-upward trend of magnetic grains (Fig. 3g). After this age this ratio begins to increase, signaling that magnetic grains become finer in the upper part

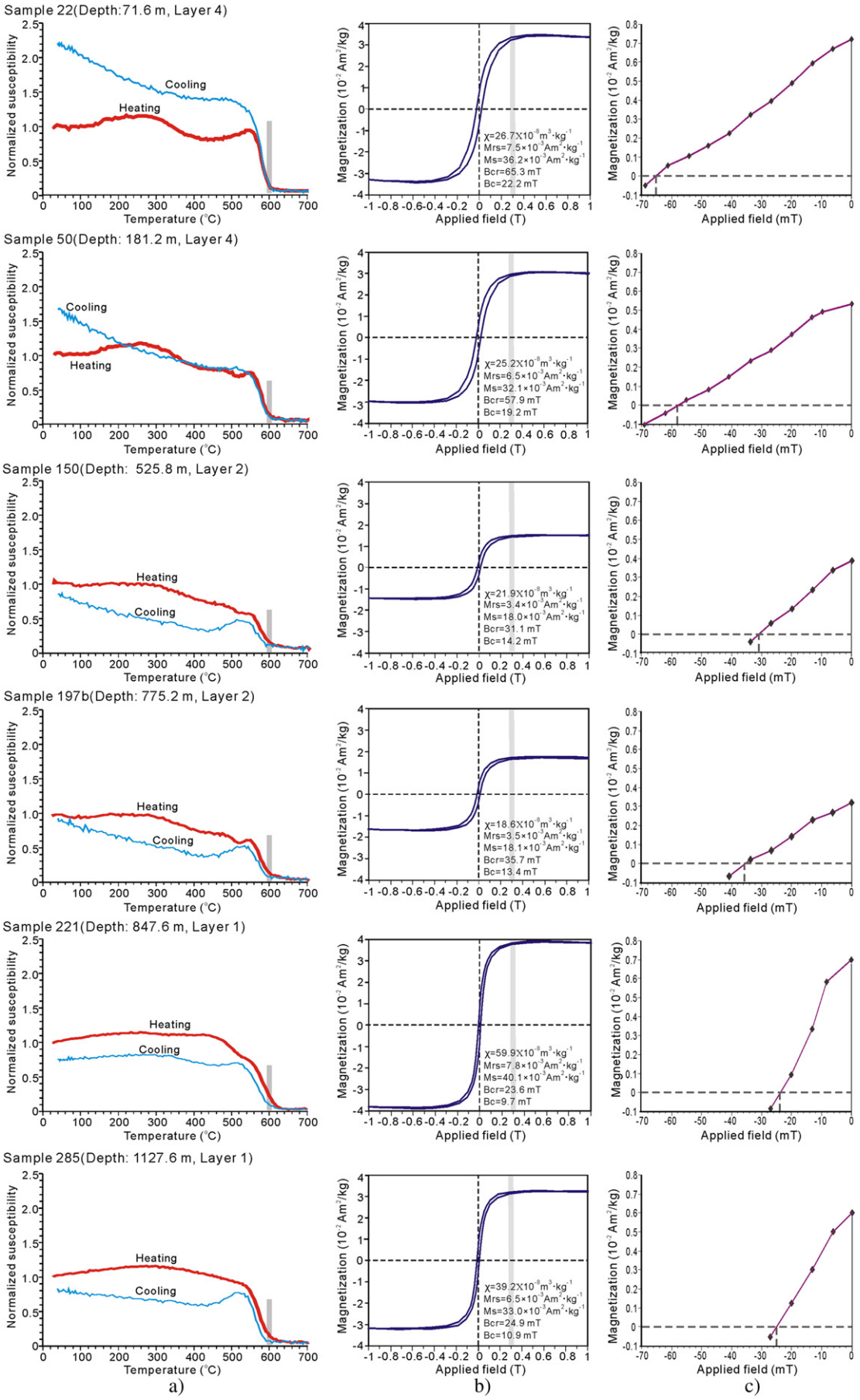

Fig. 5. (a) Thermal magnetic curves (κ–T), (b) hysteresis loops, and (c) IRM demagnetization curves for representative samples in the Taxi He section.

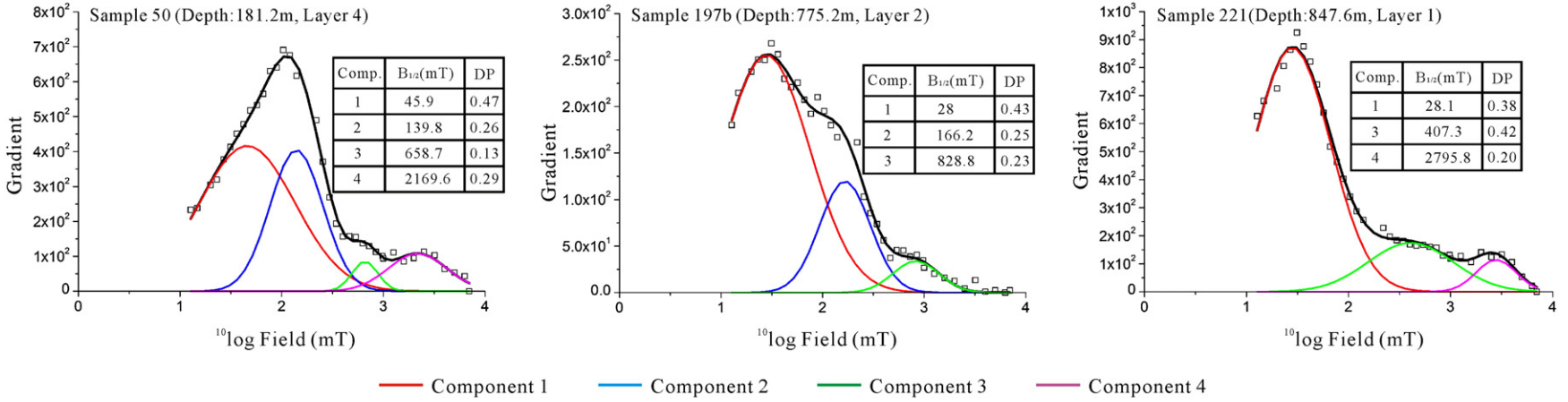

Fig. 6. IRM component analyses of representative samples from the Taxi He section, which enable four components to be identified, i.e., a low-coercivity (red, component 1) and a medium-coercivity (blue, component 2) component, and two high-coercivity components (green and purple, component 3 and component 4). $B_{1/2}$: mean coercivity (mT); DP: dispersion parameter (Kruiver et al., 2001). (For interpretation of the references to color in this figure legend, the reader is referred to the web version of this article.)

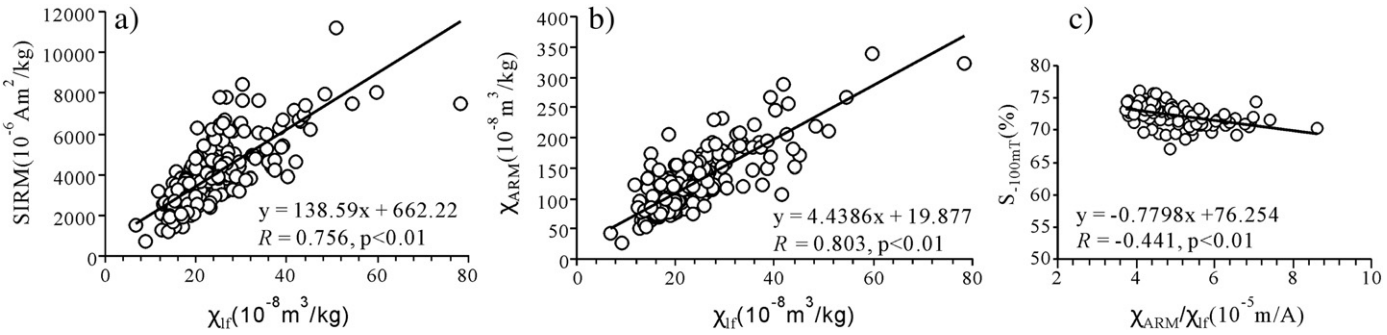

Fig. 7. Correlations between χ_{lf} and SIRM (a), χ_{lf} and χ_{ARM} (b), and S_{-100mT} and χ_{ARM}/χ_{lf} (c). In a and b, 245 samples from the whole section are analyzed, while the analysis in c is based on 104 samples from Layers 3 and 4 only.

of the Taxi He section, especially in Layer 4 (since ca. 2.7 Ma) (Fig. 3g). This variation trend of magnetic grain size is also revealed by the χ_{ARM}/SIRM ratio (Fig. 3h), the other magnetic grain size indicator, which peaks in SD range and increases with decreasing grain size (Maher, 1988). According to the significantly negative correlation between S_{-100mT} (decreasing with declining magnetic grain size) and magnetic grain size parameter χ_{ARM}/χ_{lf} (increasing with declining grain size) for samples from Layers 3 and 4 of the section (Fig. 7c), we conclude that the declining trend of S_{-100mT} values from Layer 3 towards the top of Layer 4 (Fig. 3i), a pattern opposite to that of S_{-300mT} (Fig. 3j), is likely caused both by a finer magnetic grain (Fig. 3g and h) and the presence of maghemite (Fig. 6).

5. Interpretation and discussion

5.1. Mechanism of rock magnetic property variations

In general, magnetic properties of the terrigenous deposits are controlled by sediment source, sediment particle size, mineralogy alteration during pedogenesis/diagenesis processes in the source area and subsequent transport and depositional process (e.g., Thompson and Oldfield, 1986; Pan and Zhu, 1996; Zhang et al., 2007, 2012).

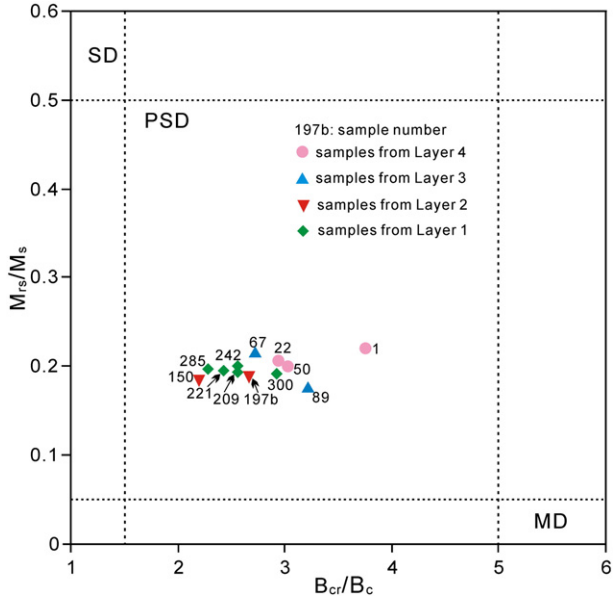

Fig. 8. Hysteresis ratios plotted on a Day plot (Day et al., 1977) for the measured samples from four layers of the section. Multidomain-MD, pseudo-single-domain-PSD and single domain-SD.

Sediment source may influence the variations in magnetic properties shown in Fig. 3. It has been demonstrated that rare earth element (REE) compositions of detrital sediments or rock are controlled mainly by sediment source material, and less influenced by sorting and diagenesis during the transport and depositional process (e.g., Taylor and McLennan, 1985; Rollinson, 1993). According to chondrite-normalized patterns of rare earth elements (REEs) of nineteen samples from the Taxi He section (Fig. 9), the REEs' compositions throughout the section are rather similar. This comparable REE composition pattern (Fig. 9) is indicative of a stable source area of the Neogene Taxi He deposits during the last several million years, hence unlikely causing such striking variations in rock magnetic properties observed in the section (Fig. 3).

Sediment particle size (related to lithofacies) is another possible factor to explain the variations of magnetic properties. As shown in Fig. 3g and h, magnetic grains display a long-term coarsening-upward trend indicated by the χ_{ARM}/χ_{lf} and χ_{ARM}/SIRM ratios in Layers 1 to 2 of the Taxi He section. In contrast, the subsequent sediments in the Taxi He section are characterized by finer magnetic grains indicated by these two ratios (Fig. 3g and h). Obviously, the finer magnetic grain since ca. 3.7 Ma, especially in Layer 4, is in correspondence with a higher content of silt fraction and a lower content of sand fraction, when compared to the previous alluvial sediments in the Taxi He section (Fig. 10b and c). This inference is further confirmed by the correlation analyses between magnetic grain size parameters and sediment particle size parameters (Fig. 4d to i). As shown in Fig. 4d and g, no or weak correlation is observed between magnetic grain size parameters (χ_{ARM}/χ_{lf} and χ_{ARM}/SIRM ratios) and clay fraction (<4 μm) of sediments. However, significant correlations exist between these two ratios and silt fraction (4–63 μm) and sand fraction (>63 μm), with the former being positive (Fig. 4e and h) and the latter negative (Fig. 4f and i). These relationships suggest that, for the analyzed samples, coarser sediments with higher sand content are characterized by coarser magnetic grains, and vice versa. In contrast to the positive relationships between χ_{ARM}, χ_{ARM}/χ_{lf}, χ_{ARM}/SIRM and the 4–63 μm fraction, the relationships between sediment particle size and χ_{lf}, χ_{fd}, SIRM, and S_{-300mT} are weak or insignificant (Table 1), implying that these magnetic parameters are not strongly influenced by particle size composition. Therefore, the change of sediment particle size composition plays a key role in the observed variations of χ_{ARM}, χ_{ARM}/χ_{lf} and χ_{ARM}/SIRM, but not other magnetic parameters (Table 1, Fig. 4).

Since sediment source and particle size cannot explain the magnetic mineral assemblage variations (as reflected by S_{-100mT} and S_{-300mT}), mineral alteration during pedogenesis and transport and depositional processes cannot be neglected. These processes can be modulated by climate change as well as tectonism. Post-depositional reductive diagenesis of magnetic minerals is driven by organic matter degradation. Normally finer sediments contain higher organic matter, and diagenesis leads to a gray color indicative of reducing condition. However, the whole Taxi He section is generally brownish in color, even in the

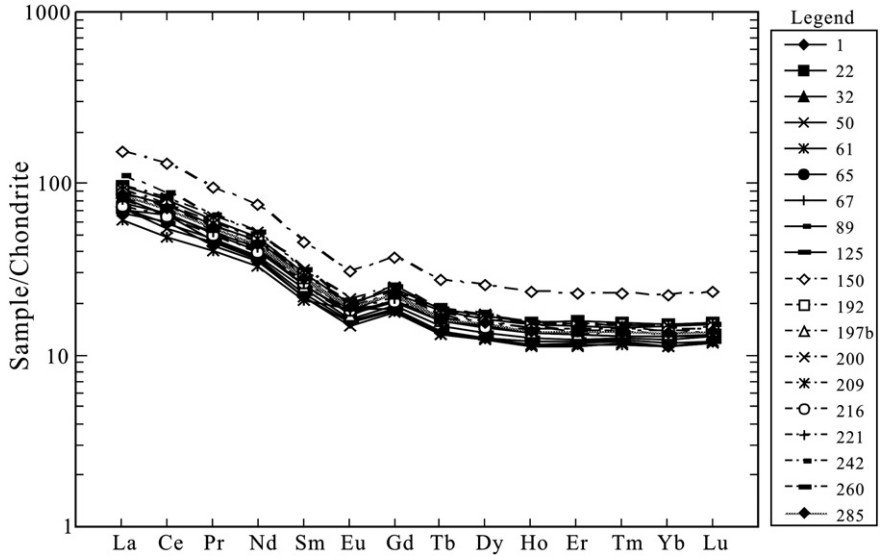

Fig. 9. Chondrite-normalized patterns of rare earth elements (REEs) of the Taxi He bulk sediments, indicating that the REEs' compositions throughout the Taxi He section are comparable and do not display a systematic variation. Chondrite data are from Taylor and McLennan (1985).

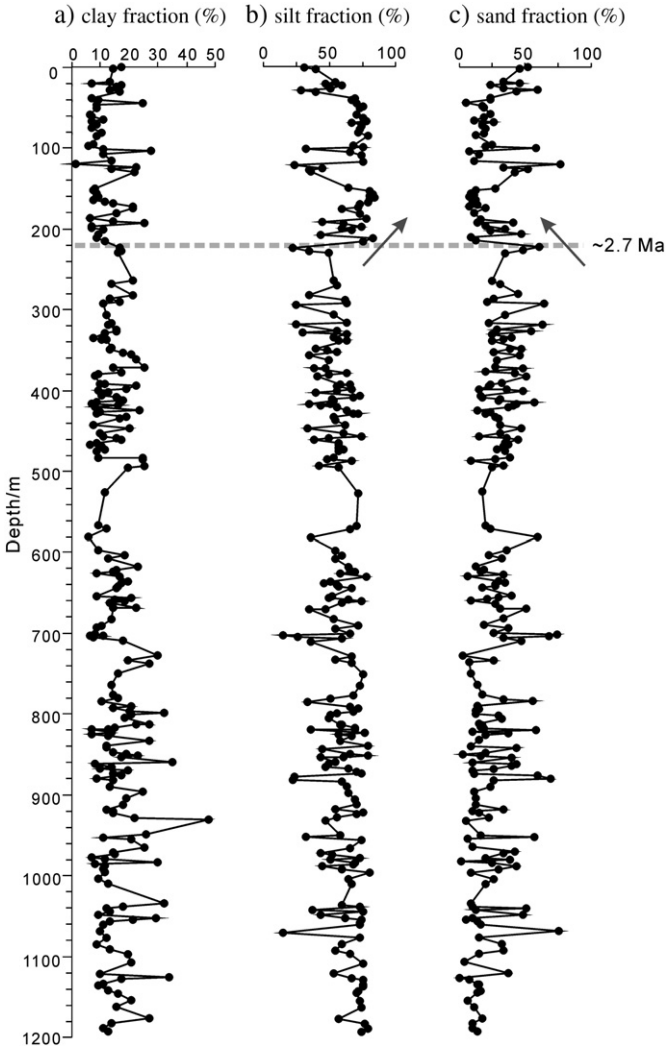

Fig. 10. Sediment particle size composition variation of the Taxi He section. (a) Clay fraction (<4 μm), (b) silt fraction (4–63 μm), and (c) sand fraction (>63 μm). For the analyzed samples, sand fraction increases upward till ca. 2.7 Ma but silt fraction decreases in this part of the section. At ca. 2.7 Ma, silt fraction significantly increases while sand fraction clearly drops.

lower fine-grained shallow lacustrine deposits (Fig. 2a, b, c and d), and the upper part of the section (Layer 3 and 4) is primarily composed of gravels and sands. Therefore, reductive diagenesis influence is expected to be minor in the Neogene Taxi He sediments. χ_{fd}% is indicative of ultrafine ferromagnetic SP grains (Thompson and Oldfield, 1986; Dearing, 1999), which is normally produced in soil pedogenesis and hence chemical weathering (Zhang et al., 2012). In the study of eolian deposits of Chinese loess, higher χ_{fd}% generally indicates a stronger pedogenesis and therefore warm and wet climate (Zhou et al., 1990). In the southern Tian Shan foreland, this parameter has also been used to indicate climate condition (e.g., Huang et al., 2010). The quite low χ_{fd}% value of the Neogene Taxi He sediments (Fig. 3d) means weak chemical weathering, which is consistent with the dominance of physical weathering at the present study area. However, ferrimagnetic mineral oxidation due to a dry condition is considerable. The higher Bcr (Figs. 5, 6 and 8) and lower S_{-100mT} (Fig. 3i) values in the upper part of the Taxi He section suggests a higher proportion of maghemite (see Section 4.1). Maghemite is an intermediate product during either ferrihydrite to hematite or magnetite to hematite alteration (Cornell and Schwertmann, 2003; Torrent et al., 2006). Since chemical weathering is weak in the study area (indicated by χ_{fd}%), we favor magnetite oxidation as the primary pathway for hematite production. The generation of maghemite by oxidation of magnetite has also been proposed in previous studies to explain the variations of χ in nearby regions (e.g., Zhang et al., 2012). It is well established that hematite production is favored in warm and dry conditions (Cornell and Schwertmann, 2003). Although daily temperature varies greatly at the present study area, the temperature can be generally as high as 35 °C and thus it is unlikely a limiting factor. Therefore, the process of magnetite oxidation is mainly controlled by dryness. Furthermore, under a drier condition, except for extreme events (flood), the transport and burial of sediment generally becomes longer due to weaker hydrodynamics. Together, the drier condition will lead to increased magnetite oxidation, and therefore a lower S_{-100mT} ratio.

5.2. Implications for Late Cenozoic Asian interior aridification

It has been demonstrated that (Lu et al., 2010b), at the Taxi He area in the northern Tian Shan foreland a progradational depositional system developed (a shallow lacustrine–alluvial fan system) during the last several million years, forming an upper Cenozoic coarsening-upward

Table 1
The correlation coefficients between sediment particle size fraction and rock magnetic parameters for 237 samples from the Taxi He section.

	χ_{lf}	χ_{fd}	SIRM	χ_{ARM}	χ_{ARM}/χ_{lf}	χ_{ARM}/SIRM	S_{-100mT}	S_{-300mT}
Clay fraction (<4 μm)	0.075	0.025	−0.093	0.08	−0.014	**0.176****	**0.208****	−0.049
Silt fraction (4–63 μm)	**0.128***	0.02	**0.189****	**0.422****	**0.473****	**0.304****	**−0.144***	0.024
Sand fraction (>63 μm)	**−0.151***	−0.115	**−0.139***	**−0.425****	**−0.435****	**−0.356****	0.049	−0.001

Note: Bold type indicates the significant relationships.
* $p < 0.05$.
** $p < 0.01$.

terrigenous sequence (Fig. 2). It means that an ~6-Ma transition of the sedimentary system (i.e. depositional dynamic change) caused a change of sediment particle size composition. At the present study area, such lithofacies transition has been attributed mainly to the stepwise growth of the Tian Shan range and the resulted encroachment into its foreland basins (e.g., Lu et al., 2010b).

In addition to tectonism, climate change can also contribute to the 6-Ma lithofacies transition from the shallow lacustrine to the alluvial fan system observed at the Taxi He area. Climate aridification would modulate river discharge and transport process and consequently contribute to the transition of a subaqueous environment to a subsequent subaerial environment at the study area, since water discharge, sediment transport and erosional competency of the fluvial systems within the piedmonts of the Tian Shan are closely related to the climate (Lu et al., 2010a).

The climate imprint is supported by our magnetic properties. As mentioned above, a drier condition would lead to decreased S_{-100mT} values due to stronger magnetite oxidation. In the Taxi He section, the upward decreases in magnetic parameters S_{-100mT} and S_{-300mT} between ca. 6 and 3.7 Ma (Fig. 3i and j) suggest more medium- and high-coercivity minerals in the coarse alluvial fan deposits than in the previous fine-textured shallow lacustrine sediments. In contrast to the 6–3.7 Ma variation, increased SIRM and S_{-300mT} but relatively stable S_{-100mT} values at ca. 3.7–2.7 Ma (Fig. 3e, i and j) indicate a slightly higher content of ferrimagnetic minerals, which is likely caused by weaker magnetite oxidation due to quick deposition. In the study area, a local tectonic activity has been chronologically constrained at ca. 4 Ma on the basis of the striking acceleration of sediment-accumulation rate from ~160 to ~250 m/Myr (Lu et al., 2010b). It is well-known that, during tectonically active periods, the resultant high relief favors quick surface erosion and transportation in response to high-energy river systems. Quick burial will favor the preservation of magnetite by limiting the exposure time of magnetite to oxygen. This might have to some extent caused the relatively higher proportions of ferrimagnetic minerals and thus a slight increase in magnetic parameters such as SIRM and S_{-300mT} since about 3.7 Ma in the Taxi He section (Fig. 3e and j).

Further intensified aridification trend occurred at ca. 2.7 Ma in terms of variations in magnetic grain size revealed by the χ_{ARM}/χ_{lf} and χ_{ARM}/SIRM ratios. Since ca. 2.7 Ma, magnetic grains are obviously finer in correspondence with a higher content of silt fraction and a lower content of sand fraction (Figs. 3g, h and 10), accompanying the further increased content of ferrimagnetic minerals (Fig. 3c, e and j). In the north piedmont of the Tian Shan, Pleistocene eolian loess extensively mantles several geomorphic surfaces (e.g, Deng et al., 2000; Lu et al., 2010a). In general, eolian silty sediments bear more fine detrital magnetic grains (e.g., Fang et al., 2007). Thus we propose that one possible cause for a finer magnetic grain and more ferrimagnetic minerals in Layer 4 of the Taxi He section (Fig. 3g and h) is due to the incorporation of eolian sediments into alluvial fan deposits as a result of the expansion of eolian deposition.

In summary, a generally upward decline of S_{-100mT} and χ_{fd}% indicates a long term drying process since ca. 6 Ma. A number of investigations (e.g., Sun and Zhang, 2008; Sun et al., 2008, 2009, 2010, 2011; Huang et al., 2010; Cai et al., 2012; Chang et al., 2012; Zhang et al., 2013) clearly show that a change to an arid climate occurred since around 6 Ma, and that the aridification trend was significantly intensified since ca. 2.6 Ma. In the northern Tian Shan foreland, the significant increase in the drought-tolerant herb taxa *Artemisia* and *Chenopodiaceae* is clearly indicative of the aridification since ca. 6 Ma (Sun and Zhang, 2008). The further intensified aridity trend since ca. 2.6 Ma is revealed by color index and magnetic susceptibility data in the western Tarim Basin (Sun et al., 2011). In the western Qaidam Basin, the aridity since the late Pliocene is also revealed by the vegetation change (Cai et al., 2012). This stepwise aridification process in the southern Junggar Basin, the Tarim Basin and the Qaidam Basin in northwestern China (Fig. 11a, b and c) is also documented by increased dust accumulation rates (DAR) in the Loess Plateau, northern China (Guo et al., 2002) (Fig. 11d) and North Pacific (Rea et al., 1998) (Fig. 11e), a feature consistent with the worldwide dry and cold climate trend during Late Cenozoic revealed by the global deep-sea oxygen isotope record (Zachos et al., 2008) (Fig. 11f). Our rock magnetic record is in accordance with these paleoclimate records (Fig. 11), suggesting that the magnetic signature of the Neogene Taxi He sediments is not a local signal, but rather a response to regional climate change. We thus propose that rock magnetic parameters such as S_{-100mT} and χ_{fd}% are potentially effective proxy indices for paleoclimate–environmental reconstruction in the Tian Shan foreland basins and the nearby areas.

6. Conclusions

Thermal magnetic measurements, hysteresis loops and IRM component analysis indicate that the magnetic signals in the Neogene Taxi He section (with an assigned magnetostratigraphic age of ca. 8.0–2.0 Ma) in the northern Tian Shan foreland, NW China are controlled primarily by soft and medium hard ferrimagnetic minerals (magnetite and maghemite) together with contribution from hard antiferromagnetic minerals (e.g., hematite). Low-field magnetic susceptibility χ_{lf} in the Taxi He section exhibits a drop at ca. 6.0 Ma, and approximately synchronous variations in some other parameters such as χ_{ARM}, SIRM, S_{-100mT} and S_{-300mT} are also observed in this section, which is interpreted as indicative of more magnetite-type minerals in shallow lacustrine sediments deposited before ca. 6.0 Ma. Marked changes in magnetic mineral composition occurred at ages of ca. 3.7 and 2.7 Ma according to these parameters. Magnetic grain throughout the section displays an upward-coarsening trend till ca. 3.7 Ma. The subsequent sediments in the top of the section are characterized by finer magnetic grains according to the χ_{ARM}/χ_{lf} and χ_{ARM}/SIRM ratios. The comparable compositions of rare earth elements (REEs) suggest that the source of the Neogene Taxi He deposits might be expected to have a similar provenance and thus is not regarded as a factor causing the observed variations in rock magnetic properties in the section. These variations are casually linked with climate aridification since the late Miocene, a regional climate trend in the Asian interior. Identified enhancement of aridification was chronologically constrained at ca. 6.0 and 2.7 Ma, respectively. Further comparisons between different paleoclimate records clearly indicate that magnetic parameters such as S_{-100mT} are

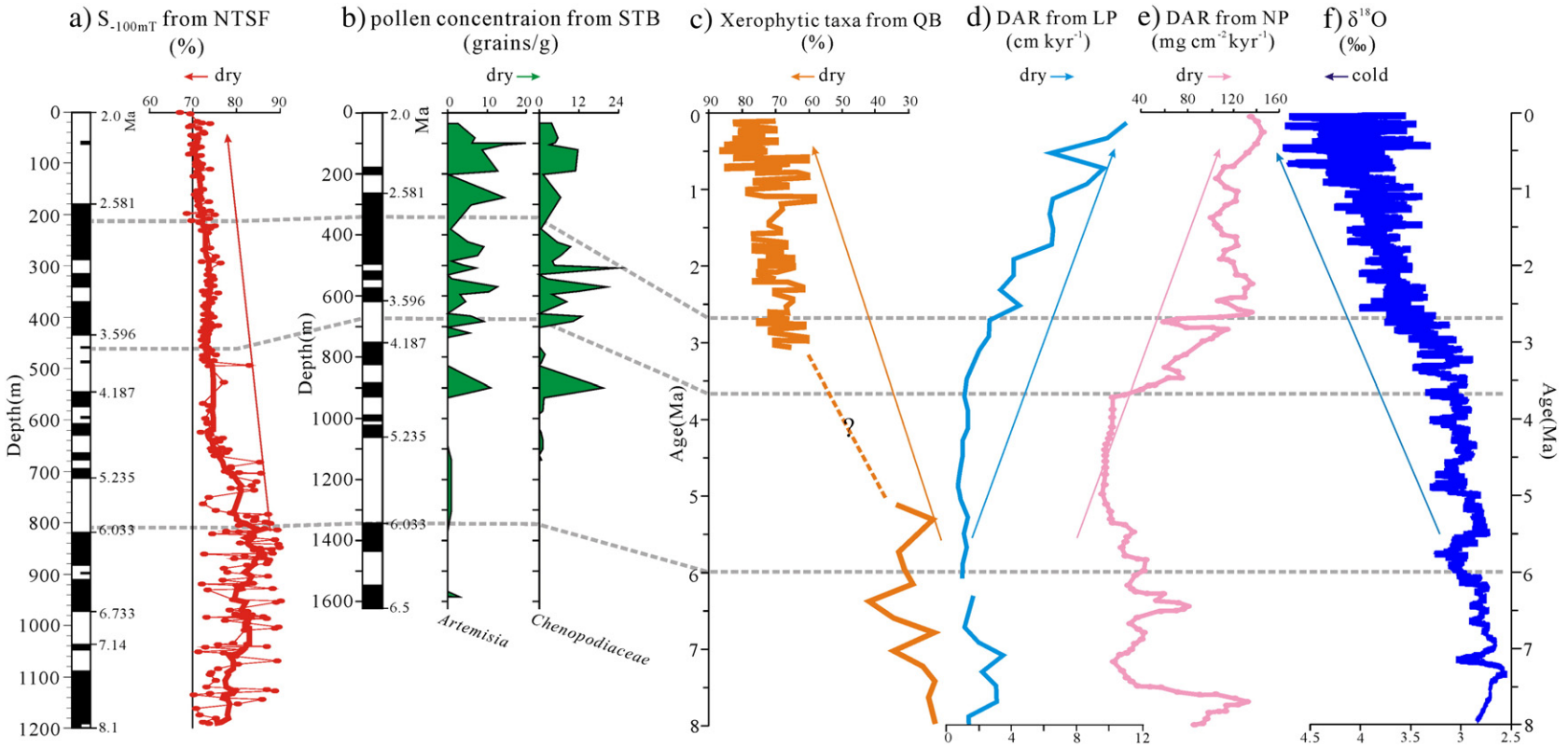

Fig. 11. A comparison of the drying record since about 6 Ma in the Taxi He section with other paleoclimate records. (a) S_{-100mT} from the northern Tian Shan foreland (NTSF) of this study; (b) pollen concentration diagram of a drought-tolerant steppe including *Artemisia* and *Chenopodiaceae* from the southern Tarim Basin (STB) (Sun et al., 2008); (c) Xerophytic taxa data from the Qaidam Basin (QB) (Miao et al., 2013); (d) dust accumulation rate (DAR) in the Loess Plateau (LP), northern China (Guo et al., 2002); (e) mass accumulation rate of eolian dust in North Pacific (NP) (Rea et al., 1998); and (f) the global deep-sea oxygen isotope record (Zachos et al., 2008).

potentially effective proxy indices for paleoclimate–environmental reconstruction in arid areas like the Tian Shan foreland basins.

Acknowledgments

This study is financially supported by the Natural Science Foundation of China (Grants 41001002 and 40971001) and China Postdoctoral Science Special Foundation (Grant 201003277). We thank Guan Wang, Honglei Ma and Ying Liu for their help in rock magnetic measurements and Lei Shao and Peijun Qiao for their assistance in geochemical analysis. We also thank Douglas W. Burbank for valuable suggestions on interpretation of magnetic susceptibility, Shouye Yang and Hao Chen for their suggestions on interpretation of geochemical data, and Xiaomin Fang and Yunfa Miao for providing us their pollen data. Valuable comments of two anonymous reviewers and the journal editor Thomas M. Cronin greatly improved the manuscript.

References

Avouac, J.-P., Tapponnier, P., Bai, M., You, H., Wang, G., 1993. Active thrusting and folding along the northern Tien Shan and late Cenozoic rotation of the Tarim relative to Dzungaria and Kazakhstan. J. Geophys. Res. 98 (B4), 6755–6804.

Banerjee, S.K., King, J., Marvin, J., 1981. A rapid method for magnetic granulometry with applications to environmental studies. Geophys. Res. Lett. 8 (4), 333–336.

Bloemendal, J., Liu, X.M., 2005. Rock magnetism and geochemistry of two Plio-Pleistocene Chinese loess–palaeosol sequences: implications for quantitative paleoprecipitation reconstruction. Palaeogeogr. Palaeoclimatol. Palaeoecol. 226 (1–2), 149–166.

Bureau of Geological and Mineral Resources of the Xinjiang Uygur Autonomous Region (BGMRX), 1993. Regional Geology of Xinjiang Uygur Autonomous Region. Geology Press, Beijing (841 pp., in Chinese).

Cai, M.T., Fang, X.M., Wu, F.L., Miao, Y.F., Appel, E., 2012. Pliocene–Pleistocene stepwise drying of Central Asia: evidence from paleomagnetism and sporopollen record of the deep borehole SG-3 in the western Qaidam Basin, NE Tibetan Plateau. Global Planet. Change 94–95, 72–81.

Chang, H., An, Z.S., Liu, W.G., Qiang, X.K., Song, Y.G., Ao, H., 2012. Magnetostratigraphic and paleoenvironmental records for a Late Cenozoic sedimentary sequence drilled from Lop Nor in the eastern Tarim Basin. Global Planet. Change 80–81, 113–122.

Charreau, J., Chen, Y., Gilder, S., Dominguez, S., Avouac, J.-P., Sen, S., Sun, D., Li, Y., Wang, W., 2005. Magnetostratigraphy and rock magnetism of the Neogene Kuitun He section (northwest China): implications for Late Cenozoic uplift of the Tianshan Mountains. Earth Planet. Sci. Lett. 230 (1–2), 177–192.

Charreau, J., Gilder, S., Chen, Y., Dominguez, S., Avouac, J.-P., Sen, S., Jolivet, M., Li, Y.A., Wang, W.M., 2006. Magnetostratigraphy of the Yaha section, Tarim Basin (China): 11 Ma acceleration in erosion and uplift of the Tian Shan Mountains. Geology 34 (3), 181–184.

Clark, M.K., House, M.A., Royden, L.H., Whipple, K.X., Burchfiel, B.C., Zhang, X., Tang, W., 2005. Late Cenozoic uplift of southeastern Tibet. Geology 33 (6), 525–528.

Cornell, R.M., Schwertmann, U., 2003. The Iron Oxides: Structure, Properties, Reactions, Occurrences and Uses, 2nd edition. Wiley-VCH, Weinheim, Germany.

Cui, Z.J., Xiong, H.G., Liu, G.N., Zhu, C., Yi, C.L., 1998. Geomorphological Process and Sedimentary Characters of the Cryosphere in the Central Tianshan Mountains. Hebei Science and Technology Publish House, Shijizhuang, China 1–305 (in Chinese).

Day, R., Fuller, M., Schmidt, V.A., 1977. Hysteresis properties of titanomagnetite: grain-size and compositional dependence. Phys. Earth Planet. Inter. 13 (4), 260–267.

Dearing, J., 1999. Magnetic susceptibility. In: Walden, J., Oldfield, F., Smith, J. (Eds.), Environmenta1 Magnetism: A Practical Guide, Technical guide, No.6, 35–62. Quaternary Research Association, London.

Deng, Q.D., Feng, X.Y., Zhang, P.Z., Xu, X.W., Yang, X.P., Peng, S.Z., Li, J., 2000. Active Tectonics of the Tian Shan Mountains. Seismology Press, Beijing 1–399 (in Chinese).

Deng, C.L., Vidic, N.J., Verosub, K.L., Singer, M.J., Liu, Q.S., Shaw, J., Zhu, R.X., 2005. Mineral magnetic variation of the Jiaodao Chinese loess/paleosol sequence and its bearing on long-term climatic variability. J. Geophys. Res. 110 (B3). http://dx.doi.org/10.1029/2004JB003451.

Dunlop, D.J., 2002. Theory and application of the Day plot (Mrs/Ms versus Hcr/Hc) 1. Theoretical curves and tests using titanomagnetite data. J. Geophys. Res. 107 (B3). http://dx.doi.org/10.1029/2001JB000486.

Dupont-Nivet, G., Krijgsman, W., Langereis, C.G., Abels, H.A., Dai, S., Fang, X.M., 2007. Tibetan plateau aridification linked to global cooling at the Eocene–Oligocene transition. Nature 445, 635–638.

Fang, X.M., Shi, Z.T., Yang, S.L., Li, J.J., Jiang, P.A., 2002. Loess sediments in the north piedmont of Tian Shan and its implication for the development of the Guerbantonggute desert. Chin. Sci. Bull. 47 (7), 540–545 (in Chinese).

Fang, X., Yan, M., Voo, R.V.D., Rea, D.K., Song, C., Parès, J.M., Gao, J., Nie, J., Dai, S., 2005. Late Cenozoic deformation and uplift of the NE Tibetan Plateau: evidence from high-resolution magnetostratigraphy of the Guide Basin, Qinghai Province, China. Geol. Soc. Am. Bull. 117 (9–10), 1208–1225.

Fang, X.M., Xu, X.H., Song, C.H., Han, W.X., Meng, Q.Q., Masayuki, T., 2007. High-resolution rock magnetic records of Cenozoic sediments in the Linxia Basin and their implications on drying of Asian Inland. Quat. Sci. 27 (6), 989–1000 (in Chinese with English abstract).

Gilder, S.A., Chen, Y., Sevket, S., 2001. Oligo-Miocene magnetostratigraphy and rock magnetism of the Xishuigou section, Subei (Gansu Province, western China) and implications for shallow inclinations in central Asia. J. Geophys. Res. 106 (B12), 30505–30521.

Guo, Z.T., Ruddiman, W.F., Hao, Q.Z., Wu, H.B., Qiao, Y.S., Zhu, R.X., Peng, S.Z., Wei, J.J., Yuan, B.Y., Liu, T.S., 2002. Onset of Asian desertification by 22 Myr ago inferred from loess deposits in China. Nature 416, 159–163.

Hu, P.X., Liu, Q.S., Torrent, J., Barrón, V., Jin, C.S., 2013. Characterizing and quantifying iron oxides in Chinese loess/paleosols: implications for pedogenesis. Earth Planet. Sci. Lett. 369–370, 271–283.

Huang, B.C., Piper, J.D.A., Qiao, Q.Q., Wang, H.L., Zhang, C.X., 2010. Magnetostratigraphic and rock magnetic study of the Neogene upper Yaha section, Kuche Depression (Tarim Basin): implications to formation of the Xiyu conglomerate formation, NW China. J. Geophys. Res. 115, B01101. http://dx.doi.org/10.1029/2008JB006175.

King, J., Banerjee, S.K., Marvin, J., Özdemir, Ö., 1982. A comparison of different magnetic methods for determining the relative grain size of magnetite in natural materials: some results from lake sediments. Earth Planet. Sci. Lett. 59 (2), 404–419.

Kirby, E., Reiners, P.W., Krol, M.A., Whipple, K.X., Hodges, K.V., Farley, K.A., Tang, W.Q., Chen, Z.L., 2002. Late Cenozoic uplift and landscape evolution along the eastern margin of the Tibetan Plateau: inferences from $^{40}Ar/^{39}Ar$ and (U–Th)/He thermochronology. Tectonics 21 (1). http://dx.doi.org/10.1029/2000TC001246.

Kruiver, P.P., Dekkers, M.J., Heslop, D., 2001. Quantification of magnetic coercivity components by the analysis of acquisition curves of isothermal remanent magnetization. Earth Planet. Sci. Lett. 189 (3–4), 269–276.

Li, J.J., Fang, X.M., 1998. Study on the uplift and environmental evolution of the Tibetan Plateau. Chin. Sci. Bull. 43 (15), 1569–1574 (in Chinese).

Li, C.X., Guo, Z.J., Meng, Z.F., Li, H.Y., Zhang, Z.C., Wu, C.D., 2006. Rock magnetic study on the Neogene sediments in the north flank of the Tian Shan. Sci. China Ser. D Earth Sci. 36 (11), 988–997 (in Chinese).

Liu, Q.S., Deng, C.L., Yu, Y., Torrent, J., Jackson, M.J., Banerjee, S.K., Zhu, R.X., 2005. Temperature dependence of magnetic susceptibility in an argon environment: implications for pedogenesis of Chinese loess/palaeosols. Geophys. J. Int. 161 (1), 102–112.

Lourens, L., Hilgen, F., Shackleton, N.J., Laskar, J., Wilson, D., 2004. The Neogene Period. In: Gradstein, F.M., Ogg, J.G., Smith, A.G. (Eds.), A Geologic Time Scale. Cambridge University Press, Cambridge, pp. 409–440.

Lu, H.J., Xiong, S.F., 2009. Magnetostratigraphy of the Dahonggou section, northern Qaidam Basin and its bearing on Cenozoic tectonic evolution of the Qilian Shan and Altyn Tagh Fault. Earth Planet. Sci. Lett. 288 (3–4), 539–550.

Lu, H.H., Burbank, D.W., Li, Y.L., 2010a. Alluvial sequence in the north piedmont of the Chinese Tian Shan over the past 550 kyr and its relationship to climate change. Palaeogeogr. Palaeoclimatol. Palaeoecol. 285 (3–4), 343–353.

Lu, H.H., Burbank, D.W., Li, Y.L., Liu, Y.M., 2010b. Late Cenozoic structural and stratigraphic evolution of the northern Chinese Tian Shan foreland. Basin Res. 22, 249–269.

Lu, H.H., Chang, Y., Wang, W., Zhou, Z.Y., 2013. Rapid exhumation of the Tian Shan range since the early Miocene: evidence from combined apatite fission track and (U–Th)/He thermochronology. Sci. China Earth Sci. (in press).

Maher, B.A., 1988. Magnetic properties of some synthetic sub-micron magnetites. Geophys. J. Int. 94 (1), 83–96.

Miao, Y.F., Herrmann, M., Wu, F.L., Yan, X.L., Yang, S.L., 2012. What controlled Mid-Late Miocene long-term aridification in Central Asia?—global cooling or Tibetan Plateau uplift: a review. Earth Sci. Rev. 112, 155–172.

Miao, Y.F., Fang, X.M., Wu, F.L., Cai, M.T., Song, C.H., Meng, Q.Q., Xu, L., 2013. Late Cenozoic continuous aridification in the western Qaidam Basin: evidence from sporopollen records. Clim. Past 9, 1485–1508.

Molnar, P., Tapponnier, P., 1975. Cenozoic tectonics of Asia: effects of a continental collision. Science 189, 419–426.

Najman, Y., Pringle, M., Godin, L., Oliver, G., 2001. Dating of the oldest continental sediments from the Himalayan foreland basin. Nature 410 (6825), 194–197.

Pan, Y.X., Zhu, R.X., 1996. The progress of environmental magnetism. Prog. Geophys. 11 (4), 87–99 (in Chinese with English abstract).

Rea, D.K., Snoeckx, H., Joseph, L.H., 1998. Late Cenozoic eolian deposition in the North Pacific: Asian drying, Tibetan uplift, and cooling of the northern hemisphere. Paleoceanography 13 (3), 215–224.

Robinson, S.G., Sahota, J.T., 2000. Rock-magnetic characterization of early, redoxomorphic diagenesis in turbiditic sediments from the Madeira Abyssal Plain. Sedimentology 47 (2), 367–394.

Rollinson, H.R., 1993. Using Geochemical Data: Evaluation, Presentation, Interpretation. Longman Scientific Technical, New York.

Shao, L., Li, A., Wu, G.X., Li, Q.Y., Liu, C.L., Qiao, P.J., 2010. Evolution of sedimentary environment and provenance in Qiongdongnan Basin in the northern South China Sea. Acta Petrol. Sin. 31 (4), 548–552 (in Chinese with English abstract).

Sun, J.M., Zhang, Z., 2008. Palynological evidence for the Mid-Miocene Climatic Optimum recorded in Cenozoic sediments of the Tian Shan Range, northwestern China. Global Planet. Change 64, 53–68.

Sun, J.M., Zhu, R.X., An, Z.S., 2005. Tectonic uplift in the northern Tibetan Plateau since 13.7 Ma ago inferred from molasse deposits along the Altyn Tagh Fault. Earth Planet. Sci. Lett. 235 (3–4), 641–653.

Sun, J.M., Zhang, L., Deng, C., Zhu, R., 2008. Evidence for enhanced aridity in the Tarim Basin of China since 5.3 Ma. Quat. Sci. Rev. 27, 1012–1023.

Sun, J.M., Zhang, Z., Zhang, L., 2009. New evidence on the age of the Taklimakan Desert. Geology 37 (2), 159–162.

Sun, J.M., Ye, J., Wu, W., Ni, X., Bi, S., Zhang, Z., Liu, W., Meng, J., 2010. Late Oligocene–Miocene mid-latitude aridification and wind patterns in the Asian interior. Geology 38 (6), 515–518.

Sun, D.H., Bloemendal, J., Yi, Z.Y., Zhu, Y.H., Wang, X., Zhang, Y.B., Li, Z.J., Wang, F., Han, F., Zhang, Y., 2011. Palaeomagnetic and palaeoenvironmental study of two parallel sections of late Cenozoic strata in the central Taklimakan Desert: implications for the desertification of the Tarim Basin. Palaeogeogr. Palaeoclimatol. Palaeoecol. 300 (1–4), 1–10.

Taylor, S.R., McLennan, S.M., 1985. The Continental Crust: Its Composition and Evolution. Blackwell, Oxford.

Thompson, R., Oldfield, F., 1986. Environmental Magnetism. Allen and Unwin, London 227.

Torrent, J., Barrón, V., Liu, Q.S., 2006. Magnetic enhancement is linked to and precedes hematite formation in aerobic soil. Geophys. Res. Lett. 33 (2). http://dx.doi.org/10.1029/2005GL024818 L02401.

Yamazaki, T., 2009. Environmental magnetism of Pleistocene sediments in the North Pacific and Ontong–Java Plateau: temporal variations of detrital and biogenic components. Geochem. Geophys. Geosyst. 10 (7), Q07Z04. http://dx.doi.org/10.1029/2009GC002413.

Yamazaki, T., Ikehara, M., 2012. Origin of magnetic mineral concentration variation in the Southern Ocean. Paleoceanography 27 (2), PA2206. http://dx.doi.org/10.1029/2011PA002271.

Yu, L.Z., Oldfield, F., 1989. A multivariate mixing model for identifying sediment source from magnetic measurements. Quat. Res. 32 (2), 168–181.

Zachos, J.C., Dichens, G.D., Zeebe, R.E., 2008. An early Cenozoic perspective on greenhouse warming and carbon-cycle dynamics. Nature 451, 279–283.

Zhang, Y.L., 1981. Loess sediments in the north piedmont of Tian Shan. Xinjiang Geol. 42 (1), 21–39 (in Chinese, with English abstract).

Zhang, P.Z., Deng, Q.D., Yang, X.P., Peng, S.Z., Xu, X.W., 1996. Late Cenozoic tectonic deformation and mechanism along the Tianshan Mountain, Northwestern China. Earthquake Res. China 12 (2), 127–140 (in Chinese with English abstract).

Zhang, W.G., Dai, X.R., Zhang, F.R., Shi, Y.X., Yu, L.Z., Dearing, J.A., 2007. Magnetic properties of sediments from the Chaohu Lake for the last 7000 years and their implications for the evolution of Asia Monsoon. Quat. Sci. 27 (6), 1053–1062 (in Chinese with English abstract).

Zhang, W.G., Yu, L.Z., Lu, M., Zheng, X.M., Ji, J.F., Zhou, L.M., Wang, X.Y., 2009. East Asian summer monsoon intensity inferred from iron oxide mineralogy in the Xiashu Loess in southern China. Quat. Sci. Rev. 28, 345–353.

Zhang, W.L., Appel, E.W., Fang, X.M., Yan, M.D., Song, C.H., Cao, L.W., 2012. Paleoclimatic implications of magnetic susceptibility in Late Pliocene–Quaternary sediments from deep drilling core SG-1 in the western Qaidam Basin (NE Tibetan Plateau). J. Geophys. Res. 117. http://dx.doi.org/10.1029/2011JB008949 B06101.

Zhang, Z.G., Han, W.X., Fang, X.M., Song, C.H., Li, X.Y., 2013. Late Miocene–Pleistocene aridification of Asian inland revealed by geochemical records of lacustrine-fan delta sediments from the western Tarim Basin, NW China. Palaeogeogr. Palaeoclimatol. Palaeoecol. 377, 52–61.

Zheng, H., Powell, C.M., An, Z., Zhou, J., Dong, G., 2000. Pliocene uplift of the northern Tibetan Plateau. Geology 28 (8), 715–718.

Zhou, L.P., Oldfield, F., Wintle, A.G., Robinson, S.G., Wang, J.T., 1990. Partly pedogenic origin of magnetic variations in Chinese loess. Nature 346, 737–739.

Zhu, B., 2005. Paleomagnetism: Basis, Principle, Method and Application. Science and Technology Publish House, Beijing, pp. 12–13, pp. 182–187 (in Chinese).

Zuo, T.W., Cheng, H.J., Liu, P., Xie, F., Deng, C.L., 2012. Magnetostratigraphic dating of the Hougou Paleolithic site in the Nihewan Basin, North China. Sci. China Ser. D Earth Sci. 54 (11), 1643–1650.